

Influence of Polydispersity on Random Sequential Adsorption of Spherical Particles

ZBIGNIEW ADAMCZYK,¹ BARBARA SIWEK, MARIA ZEMBALA, AND PAWEŁ WEROŃSKI

Institute of Catalysis and Surface Chemistry, Polish Academy of Sciences, 30-239 Cracow, ul.Niezapominajek 1, Poland

Random sequential adsorption (RSA) of polydisperse mixtures of hard and interacting spherical particles was analyzed. Theoretical results were derived by performing numerical MC simulations both for Gaussian and for continuous distributions of particle sizes characterized by standard deviations below 20%. Adsorption kinetics of these mixtures was determined for a broad range of times showing that for $\tau < 5$ the influence of polydispersity was rather minor for both Gauss and continuous particle size distributions. More significant deviations were predicted for the asymptotic adsorption regime close to jamming. In the case of continuous distributions this limiting kinetics could be described by the power law dependence $\theta_\infty - \theta \sim \tau^{-1/3}$ in accordance with the predictions of G. Tarjus and J. Talbot (1991, J. Phys. Math Gen. 24, L913). The jamming concentration θ_∞ for hard (noninteracting) particles was found to increase proportionally to $\bar{\sigma}$. It was also shown that the polydispersity of particle mixtures can exert an effect on the structure of the adsorption layer (characterized in terms of the pair correlation function). The broadening of this function was confirmed experimentally by using colloid suspensions of spherical particles (polystyrene latex) characterized by $\bar{\sigma} = 6\text{--}10\%$. © 1997 Academic Press

Key Words: adsorption on polydisperse particles; kinetics of particle adsorption; localized adsorption; irreversible adsorption; RSA of polydisperse mixtures.

Adsorption of colloid and bioparticles is of a large practical significance for polymer and colloid science, biophysics, and medicine, enabling better control of protein and cell separation processes (e.g., by filtration and chromatography), enzyme immobilization, thrombosis, biofouling of transplants and artificial organs, etc.

It has been experimentally observed (1–4) that adsorption of bioparticles and colloids is an essentially irreversible and localized process. Consequently, adsorption kinetics, the jamming limit, and the structure of adsorbed layers can be analyzed in terms of various random sequential adsorption (RSA) models developed originally for hard monodisperse particles of various shapes such as spheres (more precisely disks) (5–7), cubes (squares) (8, 9), cylinders (rectangles) (10), spherocylinders (11, 12), and spheroids (ellipses)

(11–13). These models are expected to describe real situations only when the electrostatic interactions among adsorbed and adsorbing particles (called often lateral interactions) are effectively reduced due to the addition of concentrated electrolytes.

In general, however, these electrostatic interactions play a significant role in influencing both the kinetic and the structural aspects of colloid particle adsorption (3, 4). Then, more elaborate RSA models, using the effective hard particle concept, become appropriate (14, 15).

Experiments verifying the theoretical predictions stemming from the RSA and related models were performed using colloid particle suspensions in micrometer size ranges suitable for direct microscope observations (3, 4). These involved polystyrene latexes of negatively and positively charged particles (14, 16–17) or melamine latex of amphoteric character (18, 19). Although the main features of the RSA model were confirmed, no estimation was done on the role of polydispersity of the colloid suspensions, which was of the order of 5–15% (expressed in terms of the standard deviation σ of the corresponding particle size distribution).

It also seems that few theoretical works were devoted to this subject. The existing ones focused mostly on modeling the behavior of polydisperse mixtures of hard disks, which can effectively be treated as two-dimensional.

Thus, Talbot and Schaaf (20) theoretically analyzed adsorption of two-component mixtures of disks widely differing in diameter. Both adsorption kinetics and the jamming limit of larger disks (in the limit when the size of the smaller decreased to zero) were determined.

Meaken and Jullien (21) performed extensive RSA simulations of adsorption kinetics and jamming limit for polydisperse disks characterized by bimodal, uniform, and truncated Gauss size distributions. Their calculation seemed to confirm the theoretical conjecture of Tarjus and Talbot (22), who predicted, by performing an asymptotic analysis, that the jamming coverages θ_∞ for polydisperse mixtures with uniform size distribution should be approached according to the power law dependence; i.e.,

$$\theta_\infty - \theta \sim \tau^{-1/3}, \quad [1]$$

¹ To whom correspondence should be addressed. Fax: (48 12) 251923; E-mail: ncadamcz@cyf-kr.edu.pl.

where $\theta_\infty = \pi\bar{a}^2N_\infty$ (\bar{a} is the average particle radius, N_∞ is the jamming surface concentration of adsorbed particles), $\theta = \pi\bar{a}^2N$ is the dimensionless surface coverage for a given dimensionless adsorption time τ to be defined later. However, the dependence of θ_∞ on the polydispersity parameter (width of the corresponding particle size distribution) was not determined.

Muralidhar and Talbot (23) used the moment method to describe reversible adsorption of polydisperse disks and spheres in the limit of low coverages when the surface blocking parameter (available surface function) of a given component was approximated by the Langmuir model.

In view of the limited number of results (practically non-existing for interacting spheres), it seemed interesting to perform numerical simulations aimed at a quantitative evaluation of the role of polydispersity in particle adsorption phenomena, the main goal of this work. Both the kinetics and the structure of adsorbed layers should be considered. Since in the experiments the σ value rarely exceeds 20%, in the calculations discussed hereafter we focus our attention on this range of the polydispersity parameter.

THE SIMULATION METHOD

The basic assumptions of the RSA model used in our calculations were (3–7): (i) the interface at which particles adsorb is homogeneous on a microscopic scale; (ii) if an adsorbing particle overlaps with any preadsorbed particle, it is rejected with unit probability; (iii) otherwise, the particle will be adsorbed at a given point over the target with the probability calculated from the Boltzmann distribution; once the particle becomes adsorbed its position does not change (localized adsorption).

In practice, the algorithm of the numerical simulations was analogous to that developed previously for monodisperse spheres (14–17) and consisted of three main calculation modules repeated in a loop:

(i) A virtual (adsorbing) particle was created having the coordinates (x_v, y_v) expressed relative to a space-fixed coordinate system (see Fig. 1); this was achieved using a high-quality pseudo-random-number generator giving a uniform distribution of random numbers within the range 0–1 with minimum sequential correlations. Hence, the simulation plane was a square of unit length and area; at its perimeter the usual periodic boundary conditions were applied. The radius of the virtual particle a_v was chosen at random from an appropriate size distribution, i.e., either Gauss or uniform distributions characterized by the average particle size \bar{a} and the standard deviation σ_G . To facilitate further calculation steps the $z_v = a_v$ coordinate was attributed to the adsorbing particle, so the adsorption problem became quasi three-dimensional.

(ii) Then, the vicinity of the virtual particle was searched

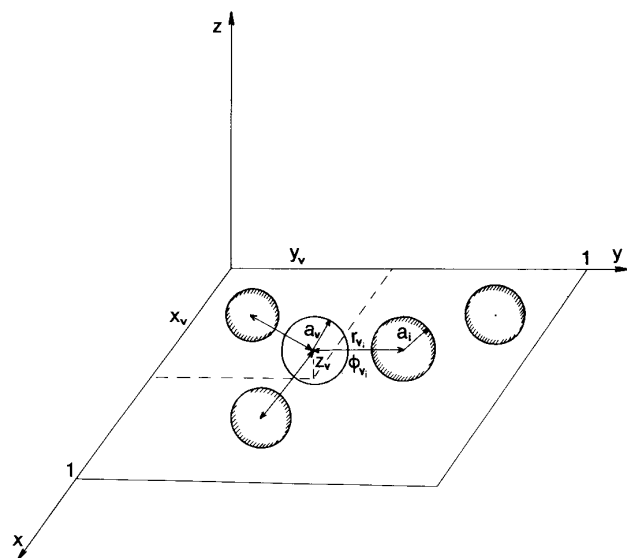


FIG. 1. A schematic representation of the RSA simulations of adsorption of polydisperse mixtures at planar interfaces.

for preadsorbed particles to determine the distances τ_{vi} (see Fig. 1); if overlapping occurred, i.e., when one of these distances was found to be smaller than $a_v + a_i$, then the virtual particle disappeared and step (i) was repeated; the number of attempts N_{att} was increased by one.

(iii) Otherwise, the probability of adsorbing the virtual particle was calculated from the Boltzmann distribution $\delta p_v = \exp(-\phi_v/kT)$ (where ϕ_v is the net interaction energy of the virtual particle with the neighboring preadsorbed particles calculated by accepting the additivity principle (3, 14), k is the Boltzmann constant, and T is the absolute temperature). For hard particles, $\phi_v = 0$ and this step was omitted. If δp_v was larger than an additional random number generated at this step (lying within the interval 0–1), then the virtual particle was adsorbed at (x_v, y_v, z_v) and its coordinates were stored. Otherwise the entire calculation loop was repeated.

To enhance the efficiency of scanning of the adsorbing particle vicinity, a subsidiary two-dimensional grid was introduced (14, 17, 21) with a mesh size equal to $1.41 a_{min}$, which ensures that the center of only one particle can lie within a particular cell (a_{min} is the minimum radius expected in simulations). Usually, for calculating adsorption kinetics about 10,000 particles were considered. The dimensionless adsorption time was calculated from the general definition (3)

$$\tau = \frac{t}{t_{ch}} = \frac{N_{att}}{N_{ch}} = \frac{\pi\bar{a}^2N_{aH}}{\theta_{ch}}, \quad [2]$$

where t_{ch} is the characteristic adsorption time and $N_{ch} =$

$\theta_{\text{ch}}/\pi\bar{a}^2$ is the characteristic surface concentration and $\theta_{\text{ch}} = 0.547$.

The maximum values of the dimensionless times τ achieved in our simulation were about 10^5 , which required 10^9 simulation steps. The jamming concentrations θ_{∞} were calculated by extrapolating the results obtained for the limiting dimensionless times, assuming power law dependencies.

The pair correlation function (radial distribution function) g_2 was determined using the equation

$$g_2(\mathbf{r}) = \frac{S}{N_t^2} \left\langle \sum_{\substack{i,j \\ i \neq j}}^N \delta_{\text{D}}[\mathbf{r} - (\tau_j - \tau_i)] \right\rangle, \quad [3]$$

where \mathbf{r} is the position vector of a point over the adsorption plane (measured from the center of an adsorbed particle), S is the surface area for which the g_2 function should be evaluated, N_t is total number of particles adsorbed over this area, δ_{D} is the Dirac delta function, \mathbf{r}_i , \mathbf{r}_j are position vectors of the i and j particle, and $\langle \rangle$ means the ensemble average.

In the absence of external forces when the system can be treated as isotropic, the vector \mathbf{r} can be replaced by the radial coordinate r and the pair correlation function can be calculated more directly by converting Eq. [3] to the form (14)

$$g_2(\mathbf{r}) = g_2(r) = \frac{S}{N_t} \frac{\bar{N}_a(r)}{2\pi r \Delta r}, \quad [4]$$

where $\bar{N}_a(r)$ is the average number of particles in the annulus of the mean radius r and the width Δr .

To attain a satisfactory accuracy of g_2 the position vectors of about 20,000 particles were considered.

RESULTS AND DISCUSSION

1. Particle Adsorption Kinetics

Most of the simulations discussed hereafter were carried out for the Gauss distribution with the probability density δp of finding a particle of radius a expressed in the usual form

$$\delta p(a) = \frac{1}{\sigma_G \sqrt{2\pi}} e^{-1/2[(a-\bar{a})/\sigma_G]^2}, \quad [5]$$

where \bar{a} is the average particle size and σ_G is the standard deviation of the distribution (see Fig. 2). The relative standard deviation of the above Gauss distribution equals $\bar{\sigma} = \sigma_G/\bar{a}$.

However, the use of the Gauss distribution in simulations may not be an advantage, especially for long simulation times, due to the finite probability of generating arbitrarily

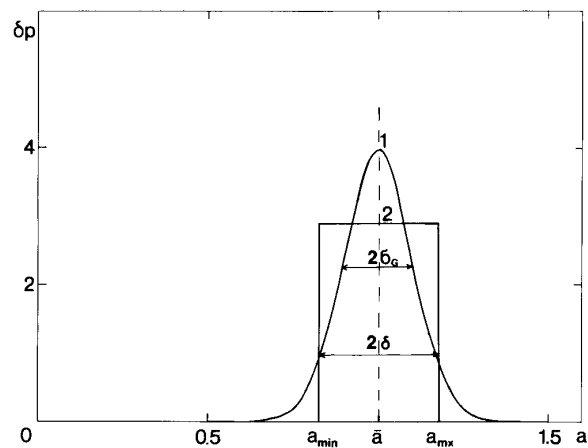


FIG. 2. The Gauss (curve 1) and the uniform (curve 2) particle size distributions having the same standard deviation of $0.1\bar{a}$.

small particle sizes. One may attempt to minimize this deficiency by truncating the Gauss distribution at a given particle size (e.g., at $\bar{a} \pm 5\sigma_G$) as done by Meakin and Jullien (21). However, this truncation limit is somewhat arbitrary and cannot be justified *a priori*. Therefore, one of the goals of our simulations was to determine the range of validity of the Gauss distribution for describing the polydispersity effect in colloid particle adsorption processes. This was achieved by comparing the results obtained for the Gauss distribution with analogous calculations performed for a uniform size distribution characterized by the same standard deviation σ_G (see Fig. 3). The probability density δp is given in this case by the simple equation

$$\delta p(a) = \frac{1}{2\sqrt{3}\sigma_G} \quad [6]$$

for $a_{\text{min}} < a < a_{\text{max}}$, where a_{min} is the minimum and a_{max} the maximum particle size, respectively; the width of the distribution $a_{\text{min}} - a_{\text{max}} = 2\delta$ is always equal to $2\sqrt{3}\sigma_G$ (see Fig. 2).

Our calculations were carried out for values of $\bar{\sigma} \leq 20\%$. For such narrow size distributions the adsorption rate constant (normalized initial adsorption flux \bar{j}_0) can be assumed independent of particle size. This is justified by the fact that for colloid particles in the micrometer size range the initial flux depends little on particle size, especially for low and moderate flow rates (3). Usually, for this particle size range the flux increase due to the interception effect is compensated by the decrease due to decreased particle diffusivity.

From an experimental viewpoint particle adsorption kinetics, i.e., the dependence of the surface coverage on the adsorption time τ , is most interesting. However, for polydisperse mixtures one can specify at least two different definitions of the dimensionless surface coverage θ .

The first is a natural extension of that used for monodisperse mixtures; i.e.,

$$\theta_p = \sum_{i=1}^{N_t} S_i N_i, \quad [7]$$

where $S_i = \pi a_i^2$ is the projection (cross section) area of the i th particle whose surface concentration (number of particles per unit area) equals N_i .

Although this definition is unequivocal physically, it has limited applicability to experimental situations since measuring the sizes of all adsorbed particles is impractical. Therefore, in experimental work one uses exclusively another definition of θ ,

$$\theta_e = \bar{S} N_t = \pi \bar{a}^2 \dot{N}_t, \quad [8]$$

where \bar{S} is the average projection area determined from the average particle size \bar{a} in the bulk, which can easily be done experimentally, e.g., by using a light-scattering method or the Coulter counter method (3).

Using these definitions one can present the simulated kinetic dependencies θ vs τ as shown in Fig. 3 for noninteracting particles (for adsorption times $\tau < 5$). As discussed in (3) the dimensionless time τ defined in computer simulations corresponds directly to the experimental adsorption time t/t_{ch} , where t is the physical adsorption time and t_{ch} is

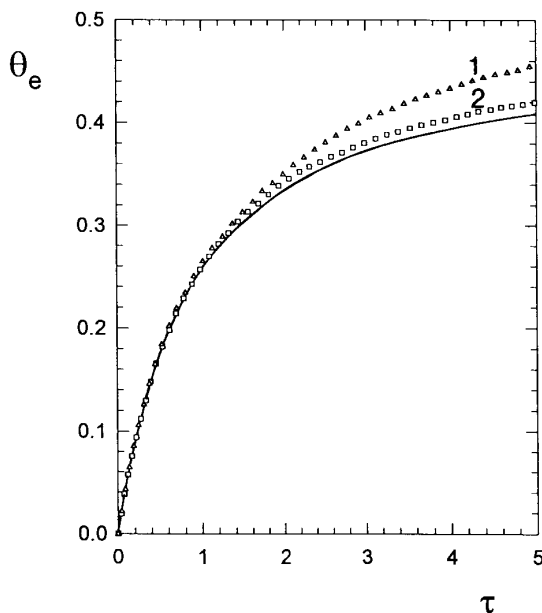


FIG. 3. Kinetics of polydisperse mixture adsorption (noninteracting particles) expressed as the dependence of θ_e on the dimensionless adsorption time τ . The points represent numerical simulations performed for the Gauss distribution characterized by the relative standard deviation σ equal: (1) $\sigma = 20\%$; (2) $\sigma = 10\%$. The continuous line shows the RSA kinetics for monodisperse particles ($\sigma = 0$).

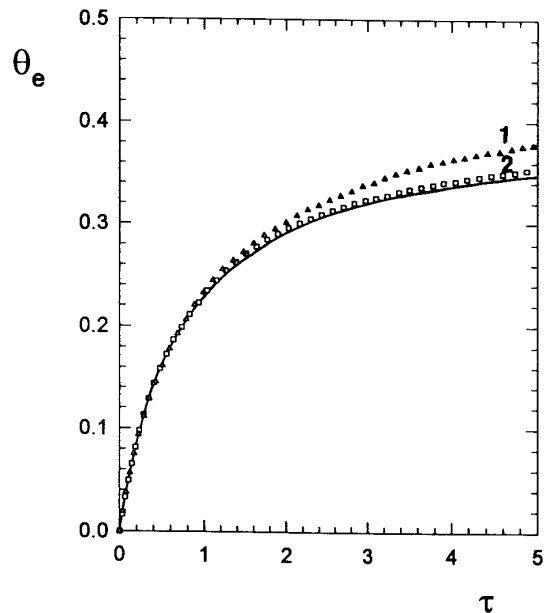


FIG. 4. Same as Fig. 2 but for interacting particles characterized by $\kappa\alpha = 25$ and $\phi_0 = 100 kT$: (1) $\sigma = 20\%$; (2) $\sigma = 10\%$. The continuous line shows the RSA kinetics for monodisperse particles ($\sigma = 0$).

the characteristic adsorption time defined as the time of forming a ‘‘monolayer’’ ($\theta_e = \theta_{\text{ch}} = 0.547$) by assuming a constant adsorption rate \bar{j}_0 ; i.e.,

$$t_{\text{ch}} = \frac{\theta_{\text{ch}}}{\pi \bar{a}^2 \bar{j}_0 n_b} \quad [9]$$

(n_b is the particle number concentration in the bulk of the suspension).

For a typical suspension of a particle $1 \mu\text{m}$ in diameter characterized by $n_b = 10^9 \text{ cm}^{-3}$ and $\bar{j}_0 = 5 \times 10^{-5} \text{ cm/s}$ one can calculate that $t_{\text{ch}} = 1390 \text{ s}$. Thus, $\tau = 1$ in Fig. 3 would correspond physically to an adsorption time of 1390 s for the above suspension.

As can be seen in Fig. 3, for $\sigma = 10\%$ the influence of the polydispersity on particle adsorption kinetics is rather minor, smaller than an experimental error. Deviations between monodisperse and polydisperse mixtures become detectable, however, for $\sigma = 20\%$ and $\tau > 2$. This is only so if one uses the empirical θ_e definition. When the proper physical definition given by Eq. [7] is used, all kinetic curves for different polydispersity parameters become practically indistinguishable.

Similar calculations performed for the interacting particles are shown in Fig. 4. As mentioned, the interactions among adsorbed and adsorbing particles were calculated using the additivity rule as a sum of the individual contributions stemming from particle pairs. Since our calculations were performed for stable colloid suspensions (aggregation ex-

cluded), the net interaction potential was assumed to be governed by the repulsive electrostatic interactions which for a pair of particles having the radii a_i and a_j were approximated by (4)

$$\phi_{ij} = \phi_0 \frac{2\bar{a}_i\bar{a}_j}{\bar{r}_{ij}} e^{-\kappa a_{ij}}, \quad [10]$$

where $\phi_0 = \frac{1}{2} \epsilon \bar{a} (kT/e)^2 Y^{0^2}$, ϵ is the dielectric constant of the solution, e is the elementary charge, $Y^0 = 4 \tanh(\psi^0 e / 4kT)$, ψ^0 is the surface potential of the particle (assumed independent of particle size), $\bar{a}_i = a_i / \bar{a}$, $\bar{a}_j = a_j / \bar{a}$, $\bar{r}_{ij} = r_{ij} / \bar{a}$ is the dimensionless radial distance between particle centers, $\bar{h}_{ij} = \bar{r}_{ij} - \bar{a}_i - \bar{a}_j$ is the minimum distance between particle surfaces, and $\kappa^{-1} = (\epsilon kT / 8\pi e^2 I)^{1/2}$ is the Debye screening length (I is the ionic strength of the solution).

Equation [10] is based on the linear superposition principle (LSA) and is applicable as discussed recently (4) to a broad range of surface potentials and κa values, provided that $\kappa a \bar{h}_{ij} > 1$.

The results shown in Fig. 4 were obtained for $\phi_0 = 100 kT$ and $\kappa \bar{a} = 25$, which is a typical range for colloid suspensions, e.g., polystyrene latexes used in various experimental studies (3, 4). Particle size distribution in these calculations was approximated by the Gauss distribution, Eq. [5]. One can note in Fig. 4 that similar to noninteracting particles the deviations from monodisperse systems become noticeable for $\sigma = 20\%$ and $\tau > 2$ only.

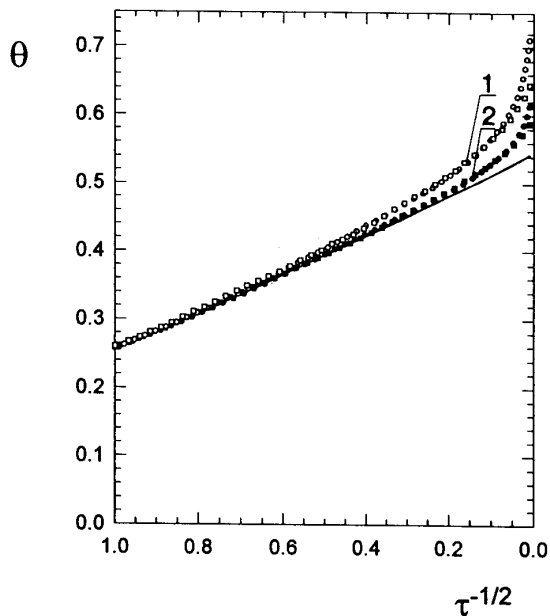


FIG. 5. Kinetics of polydisperse hard particle adsorption for long times expressed as θ vs $\tau^{-1/2}$: (1) The θ_e dependence for $\sigma = 10\%$; \circ , Gauss distribution; \square , uniform distribution. (2) The θ_p dependence for $\sigma = 10\%$; \bullet , Gauss distribution; \blacksquare , uniform distribution. The continuous line shows the RSA kinetics for monodisperse particles ($\sigma = 0$).

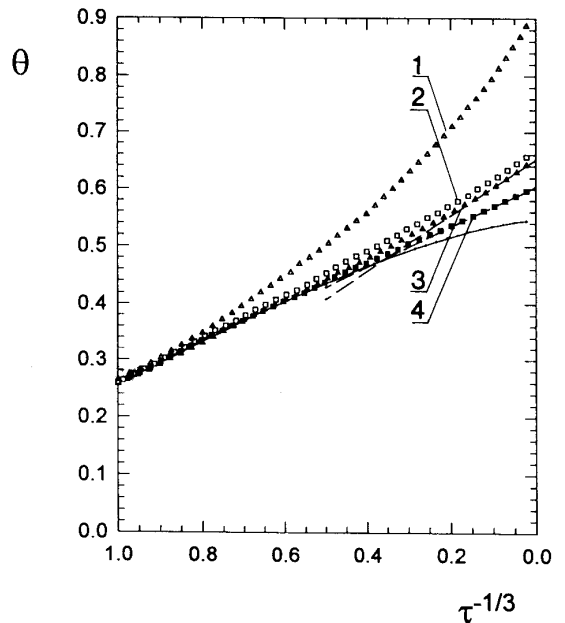


FIG. 6. Kinetics of polydisperse hard particle adsorption for long times expressed as θ vs $\tau^{-1/3}$; uniform distribution. (1) \triangle , θ_e for $\sigma = 20\%$; (2) \square , θ_e for $\sigma = 10\%$; (3) \blacktriangle , θ_p for $\sigma = 20\%$; (4) \blacksquare , θ_p for $\sigma = 10\%$. The continuous line shows the RSA kinetics for monodisperse particles, the broken lines represent the linear fit to the simulation points.

Analogous calculations were performed for the uniform particle size distribution as well. No statistically significant difference from the Gauss distribution was found for $\tau < 5$. Some deviations manifested themselves for extremely long adsorption times exceeding 10^2 . However, such long-lasting kinetic runs can only be analyzed, as suggested by previous results for monodisperse spheres (3) and Eq. [1] predicted for polydisperse systems, using the θ vs $\tau^{-1/m}$ transformation (where m equals 2 or 3), which compresses the infinite τ domain into a finite one.

In Fig. 5 the simulation data obtained for noninteracting particles are plotted using this transformation with $m = 2$. Both θ_e and θ_p are shown for the Gauss and uniform distributions characterized by the same standard deviation $\sigma = 10\%$. As can be seen for polydisperse mixtures the kinetic dependencies, especially the θ_e vs $\tau^{-1/2}$, deviate from the straight line characteristic of the asymptotic RSA kinetic of monodisperse systems (3). It should also be noted that both particle size distributions give practically the same results except for the extremely long times, i.e., $\tau > 10^2$ ($\tau^{-1/2} < 0.1$) when only the θ values calculated by using the uniform distribution seem to approach a proper jamming limit. This observation is therefore in accordance with the simulations of Meaken and Jullien (21) performed for hard disks. As mentioned, they were forced to truncate the Gauss distribution to attain a convergence to the jamming coverage.

Since the θ vs $\tau^{-1/2}$ dependencies for polydisperse systems were not rectilinear, an extrapolation to $\tau^{-1/2} \rightarrow 0$ to

derive the jamming concentrations θ_∞ was not feasible. Therefore, in accordance with the theoretical prediction of Tarjus and Talbot (22) (cf. Eq. [3]) we alternatively expressed our simulations using the θ vs $\tau^{-1/3}$ transformation. The results presented in Fig. 6 seem to confirm their conjecture, suggesting that for the uniform size distribution the simulated results (for $\bar{\sigma} = 10$ and 20%) can adequately be interpolated by straight line dependencies. It should be mentioned that the analogous linear dependence of θ on $\tau^{-1/3}$ was theoretically predicted in the case of adsorption of monodisperse nonspherical particles, e.g., spheroids (11–13, 15).

The comparison of kinetic runs shown in Fig. 6 indicates also that the use of the empirical θ_e definition (based on the average particle size taken from the bulk) is bound to introduce a considerable error, especially for $\bar{\sigma} > 10\%$. Thus, for $\tau^{-1/3} = 0.2$ ($\tau = 125$) the true physical θ_p value was 56% whereas the θ_e value was about 71% (for $\bar{\sigma} = 20\%$). This gives a relative error of about 30%, which is well above the experimental error reached in particle adsorption measurements. This discrepancy between θ_p and θ_e is caused by the different particle size distribution in the bulk and at the surface, where the smaller particles appear more frequently at long times. This is illustrated in Figs. 7 and 8, where the simulated “monolayers” of hard particles (for $\tau = 10^5$) are presented together with the corresponding particle size distributions. It can be seen that for long times the size distribution of adsorbed particles becomes nonuniform, characterized by decreased average particle sizes in comparison with initial values. The dependencies of the average radius of adsorbed particles on $\tau^{-1/3}$ are shown in Fig. 9, both for uniform and for Gauss particle size distributions (initially).

Analogous results were presented by Meakin and Jullien (21) in the case of hard disk adsorption.

The kinetic results obtained for interacting particles ($\phi_0 = 100 kT$, $\kappa a = 25$) are shown in Fig. 10. As can be observed, θ_e for polydisperse systems were significantly larger than those for monodisperse interacting particles, especially for $\tau^{-1/3} < 0.2$. In contrast to noninteracting particles, however, the dependencies of θ_e on $\tau^{-1/3}$ were not linear. It can also be seen in Fig. 8 that for $\bar{\sigma} = 10\%$ the limiting surface coverages for long times in the case of interacting polydisperse system approaches the value obtained for monodisperse hard particles, i.e., 54.7%. On the other hand, for $\bar{\sigma} = 20\%$ the kinetic curve for interacting polydisperse particles crosses that for noninteracting monodisperse particles at τ about 30.

Our simulations plotted in Fig. 10 can furnish a plausible explanation of the experimental result of Onoda and Liniger (16), who determined the jamming concentration of polystyrene latex particles (with an average diameter of $2.95 \mu\text{m}$) to be 55%. This value was in perfect agreement with the RSA

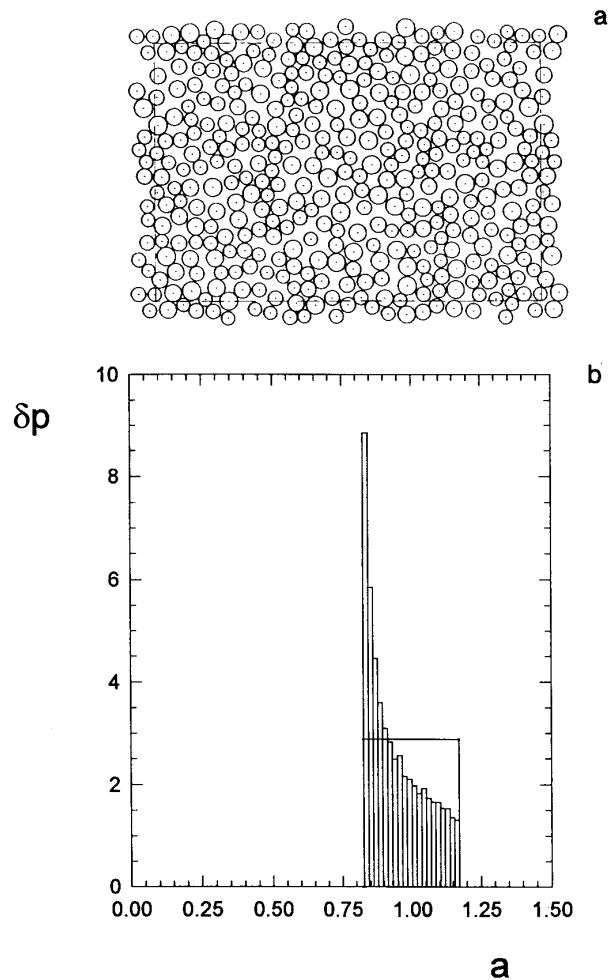


FIG. 7. (a) The monolayer of adsorbed hard polydisperse particles close to jamming limit ($\tau = 10^5$, $\theta_p = 58\%$, $\bar{\sigma} = 10\%$). (b) The corresponding size distributions, i.e., uniform initially with $\bar{a} = 1$ and finally with $\bar{a} = 0.95$.

model prediction for hard spheres, although the adsorption experiments were carried out in distilled water, i.e., at low ionic strength, probably ranging between 10^{-5} and $5 \times 10^{-5} M$ (depending on the pH of the suspension). The $\kappa \bar{a}$ was therefore contained between 35 and 15. Since the standard deviation of latex suspension is usually on the order of 10%, the experimental conditions of Onoda and Liniger seem to be fairly well matched by our numerical simulation shown in Fig. 10. One may therefore suppose that the agreement of their experimental result with theoretical simulations for monodisperse hard particle system is due to compensation of the polydispersity effect increasing θ_e and the electrostatic repulsion effect decreasing this value.

Since for the uniform size distribution the jamming concentrations can accurately be determined by extrapolation, one can produce the dependence of θ_∞ on the relative standard deviation $\bar{\sigma}$, which is of a primary experimental importance. Such plots for $\bar{\sigma}$ ranging from 0 to 20% are shown

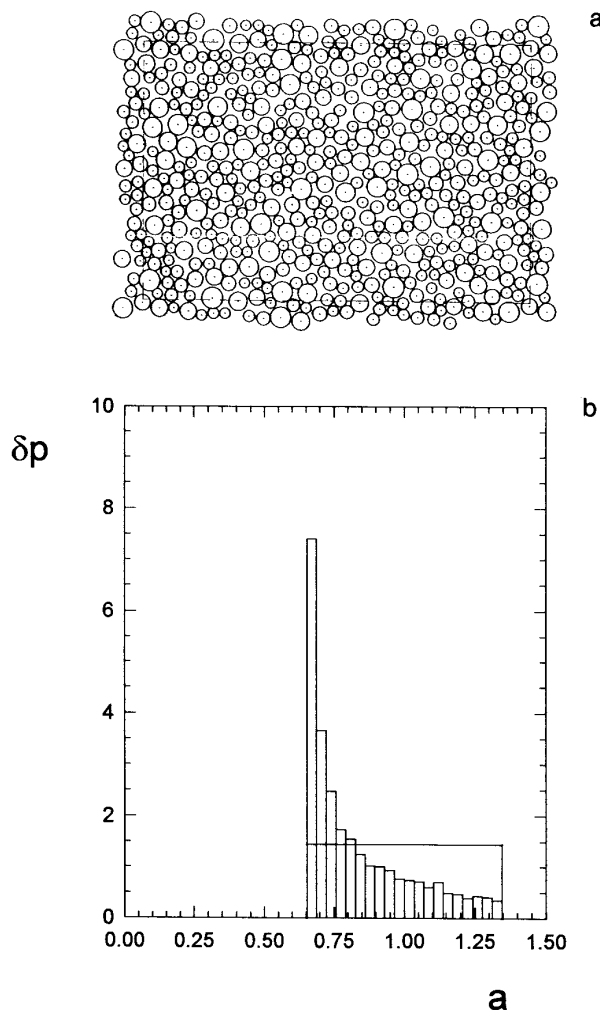


FIG. 8. Same as for Fig. 7 but for $\bar{\sigma} = 20\%$, (a) The monolayer for $\tau = 10^5$ ($\theta_p = 61\%$), (b) Particle size distributions; uniform initial with $\bar{\sigma} = 1$ and finally with $\bar{\sigma} = 0.83$.

in Fig. 11. It was found that the simulation results can be fitted for noninteracting particles by the relationships

$$\begin{aligned}\theta_{\infty p} &= 0.547 + 0.53\bar{\sigma} \\ \theta_{\infty e} &= 0.547 + 0.458\bar{\sigma} + 6.055\bar{\sigma}^2.\end{aligned}\quad [11]$$

These relationships suggest that $\theta_{\infty p}$ increases linearly with the polydispersity of a colloid suspension characterized by the standard deviation $\bar{\sigma}$, whereas $\theta_{\infty e}$ increases parabolically.

It should be noted that Meakin and Jullien (21) have determined that in the case of hard disk adsorption, θ_{∞} increased proportionally to $\bar{\sigma}^{0.86}$.

2. Structure of Adsorbed Layers

Except for the kinetic aspects discussed above the polydispersity of colloid suspensions can potentially influence the

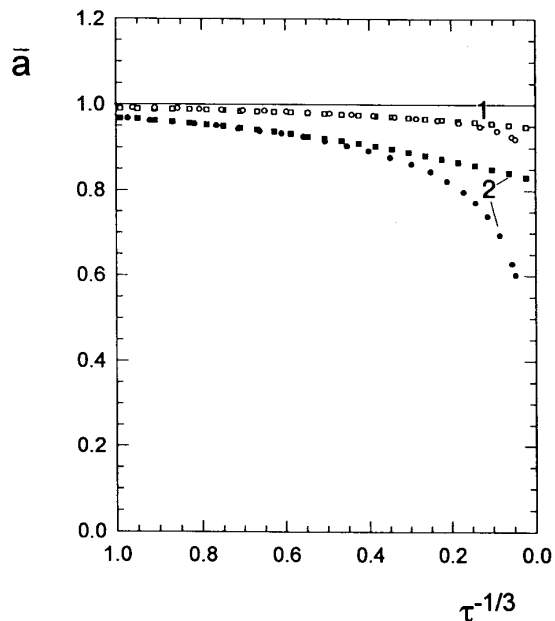


FIG. 9. The dependence of the average particle size \bar{a} on $\tau^{-1/3}$ (hard particles). (1) For $\bar{\sigma} = 10\%$; \square , uniform distribution; \circ , Gauss distribution. (2) For $\bar{\sigma} = 20\%$; \blacksquare , uniform distribution; \bullet , Gauss distribution.

structure of adsorbed layers, characterized usually in terms of the pair correlation functions g_2 . Since this function contains important information about the dynamic lateral interactions, many experimental works were undertaken to determine it for various surface coverages and ionic strengths of

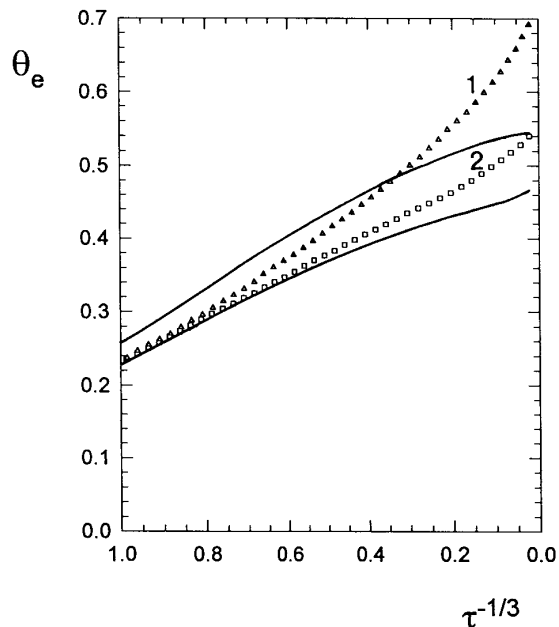


FIG. 10. Adsorption kinetics of interacting particles ($\kappa a = 25$, $\phi_0 = 100$ kT , uniform size distribution) expressed as θ_e vs $\tau^{-1/3}$. (1) Δ , $\bar{\sigma} = 20\%$. (2) \square , $\bar{\sigma} = 10\%$. The continuous lines denote the RSA results for monodisperse particles, hard (upper curve) and interacting, respectively.

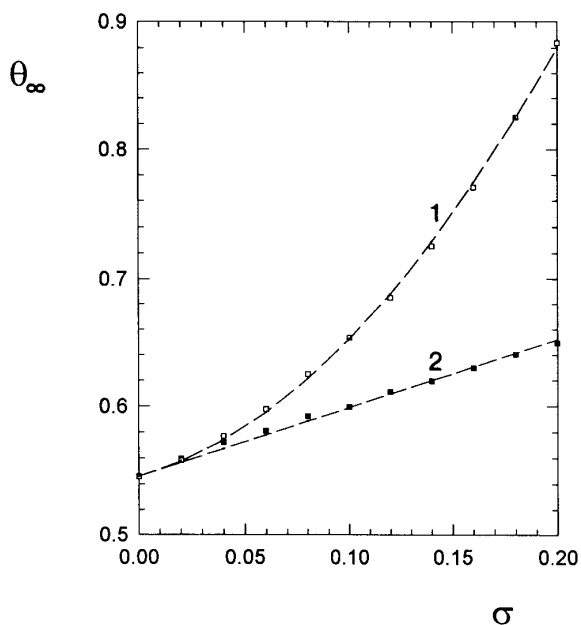


FIG. 11. The dependence of the jamming coverages θ_∞ on $\bar{\sigma}$ for polydisperse mixtures of hard particles characterized by uniform size distribution: (1) \square , θ_∞ calculated as $\pi \bar{a}^2 N_i$; (2) \blacksquare , θ_∞ calculated as $\pi \Sigma a_i^2 N_i$. The broken lines denote the best fits to the numerical data.

the suspensions (3, 4, 14, 24, 25). Yet, despite its significance no theoretical results aimed at determining the influence of particle suspension polydispersity on the shape of the pair correlation function were reported.

Such calculations performed using the RSA simulation algorithm described above are shown in Fig. 12 for two typical ionic strength values, $I = 10^{-3}$ and $I = 10^{-5}$ M. The pair correlation function was calculated according to Eq. [4]. As can be seen Fig. 12, the polydispersity effect ($\bar{\sigma} = 10\%$, Gauss distribution) caused a significant decrease in the first peak height and in the following minimum depth. Another characteristic feature of the g_2 function for polydisperse mixtures is that for distances $r/\bar{a} < 2$ its value remains larger than zero (for $I = 10^{-3}$ M) in contrast to monodisperse systems when $g_2 = 0$ for $r/\bar{a} < 2$ as a result of the nonpenetration condition.

The validity of the theoretical predictions shown in Fig. 12 was estimated by comparing them with experimental data obtained for model systems. The experiments were performed in the impinging jet cell at low Reynolds number using polystyrene latex particles of average sizes 0.88 and 1 μm , respectively, with a standard deviation of 8%. The methodology described in detail elsewhere (14) was based on the micrograph technique followed by a subsequent particle coordinate determination using a magnetic digitizer. As can be seen, the g_2 function simulated by considering particle polydispersity is in better agreement with experimental data than the previously used (14) g_2 function of monodisperse suspensions. The results shown in Fig. 12 suggest, therefore,

that the polydispersity effect can be detected more easily by measuring the pair correlation function than by performing particle adsorption kinetic experiments.

It can also be deduced from the shape of the g_2 functions that a considerable degree of a short-range ordering occurred in the adsorbed particle layers for lower ionic strength. Hence, the lateral electrostatic interactions exerted a decisive influence on the structure of adsorbed layers for suspensions characterized by low polydispersity.

CONCLUDING REMARKS

The RSA simulations performed for polydisperse suspensions have demonstrated that the changes in particle adsorption kinetics in comparison with monodisperse systems can be detected experimentally only for $\bar{\sigma} > 10\%$ and $\tau > 5$. Considerable differences between monodisperse and polydisperse systems occur at longer times, especially when the

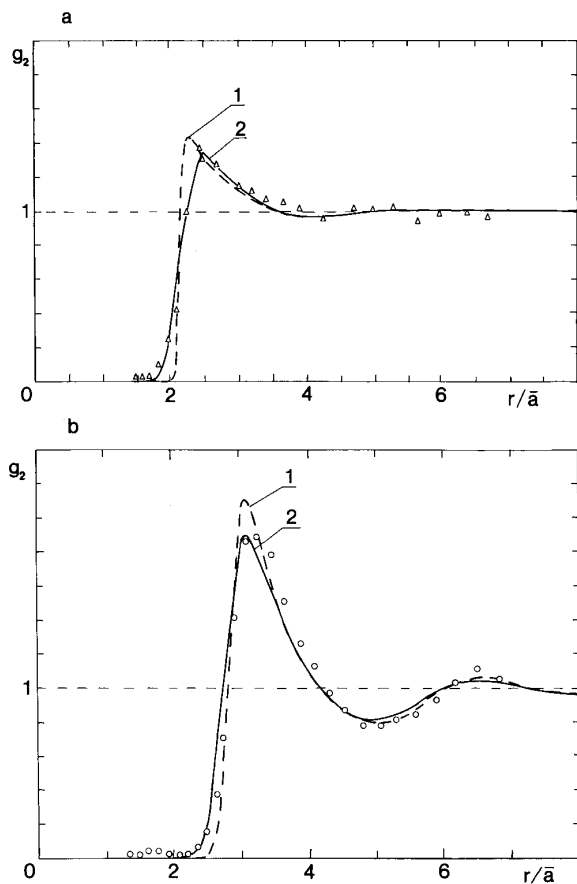


FIG. 12. The pair correlation function g_2 for interacting particles. (a) For $I = 10^{-3}$ M. The points denote experimental results obtained for polystyrene latex particles $2\bar{a} = 0.88 \mu\text{m}$, $\bar{\sigma} = 8\%$, $\theta_c = 24\%$; curves 1 and 2 denote the theoretical simulations performed for monodisperse and polydisperse particles (characterized by the Gauss distribution with the same $\bar{\sigma}$), respectively. (b) Same as (a) but for $I = 10^{-5}$ M; average particle size 1 μm ($\bar{\sigma} = 9\%$), $\theta_c = 25\%$.

empirical definition of the surface coverage $\theta_e = \pi \bar{a}^2 N_t$ is used to express adsorption kinetics. Thus, for $\sigma > 10\%$ and longer times the θ_e values calculated for polydisperse interacting particles can become larger than those for monodisperse hard particles. This suggests that the correct physical definition of $\theta_p = \pi \Sigma a_i^2 N_i$ should be used to properly express experimental data.

It was also demonstrated that both Gauss and uniform particle size distributions give the same results except for $\tau > 10^3$ when only the uniform distribution results seem to converge to a proper jamming concentration θ_∞ . The asymptotic form of the kinetic equation becomes then $\theta_\infty - \theta \sim \tau^{-1/3}$ in accordance with the conjecture of Tarjus and Talbot (22). It was demonstrated that θ_∞ increases proportionally to the polydispersity parameter σ .

Simulations of the pair correlation function g_2 showed that by considering polydispersity one can attain better agreement with the experimental data obtained for polystyrene latex suspensions characterized by $\sigma = 8\%$.

ACKNOWLEDGMENTS

This work was partially supported by the KBN, Grant 3T09 A08310.

REFERENCES

1. Feder, J., and Giaever, I., *J. Colloid Interface Sci.* **78**, 144 (1980).
2. Vincent, B., Young, C. A., and Tadros, Th. F., *J. Chem. Soc. Faraday Trans. 1* **76**, 665 (1980).
3. Adamczyk, Z., Siwek, B., Zembala, M., and Belouschek, P., *Adv. Colloid Interface Sci.* **48**, 151 (1994).
4. Adamczyk, Z., and Warszyński, P., *Adv. Colloid Interface Sci.* **63**, 41 (1996).
5. Hinrichsen, E. L., Feder, J., and Jossang, T., *J. Stat. Phys.* **11**, 793 (1986).
6. Schaaf, P., and Talbot, J., *J. Chem. Phys.* **91**, 4401 (1989).
7. Schaaf, P., and Talbot, J., *Phys. Rev. Lett.* **62**, 175 (1989).
8. Finegold, L., and Donell, J. T., *Nature* **278**, 443 (1979).
9. Viot, P., and Tarjus, G., *Europhys. Lett.* **13**, 295 (1990).
10. Vigil, R. D., and Ziff, R. M., *J. Chem. Phys.* **91**, 2599 (1989).
11. Viot, P., Tarjus, G., Ricci, S. M., and Talbot, J., *J. Chem. Phys.* **97**, 5212 (1992).
12. Ricci, S. M., Talbot, J., Tarjus, G., and Viot, P., *J. Chem. Phys.* **97**, 5219 (1992).
13. Talbot, J., Tarjus, G., and Schaaf, P., *Phys. Rev. A* **40**, 4808 (1989).
14. Adamczyk, Z., Zembala, M., Siwek, B., and Warszyński, P., *J. Colloid Interface Sci.* **140**, 123 (1990).
15. Adamczyk, Z., and Weroński, P., *Langmuir* **42**, 543 (1995).
16. Onoda, G. Y., and Liniger, E. G., *Phys. Rev. A* **33**, 715 (1986).
17. Adamczyk, Z., Siwek, B., and Zembala, M., *J. Colloid Interface Sci.* **151**, 351 (1992).
18. Adamczyk, Z., Siwek, B., and Zembala, M., *Colloids Surf.* **76**, 115 (1993).
19. Wojtaszczyk, P., Schaaf, P., Senger, B., Zembala, M., and Voegel, J. C., *J. Chem. Phys.* **99**, 7198 (1993).
20. Talbot, J., and Schaaf, P., *Phys. Rev. A* **40**, 422 (1989).
21. Meakin, P., and Jullien, R., *Phys. Rev. A* **46**, 2029 (1992).
22. Tarjus, G., and Talbot, J., *J. Phys. Math. Gen.* **24**, L913 (1991).
23. Muralidhar, R., and Talbot, J., *AIChEJ.* **39**, 1322 (1993).
24. Sjollema, J., and Busscher, H. J., *Colloid Surf.* **47**, 323 (1992).
25. Meinders, J. M., Noordmans, J., and Busscher, H. J., *J. Colloid Interface Sci.* **152**, 265 (1992).